Observation of a Metallic Antiferromagnetic Phase and Metal to Nonmetal Transition in $Ca_3Ru_2O_7$

G. Cao, S. McCall, and J. E. Crow
National High Magnetic Field Laboratory, Florida State University, Tallahassee, Florida 32306

R. P. Guertin*
Physics Department, Tufts University, Medford, Massachusetts 02155
(Received 30 September 1996; revised manuscript received 20 December 1996)

Single crystal $Ca_3Ru_2O_7$ shows a metallic antiferromagnetic phase intermediate between a first-order metal to nonmetal transition at $T_M = 48$ K and the antiferromagnetic ordering (Néel) temperature, $T_N = 56$ K. The metallic antiferromagnetic phase is predicted within various Mott-Hubbard models. Magnetization and electrical resistivity reveal strongly anisotropic metamagnetism in the nonmetallic antiferromagnetic phase. The charge and spin excitations are strongly coupled: The H-T phase diagrams determined by magnetization and magnetoresistivity are indistinguishable and reveal a multicritical point. The heat capacity of $Ca_3Ru_2O_7$ suggests it is a highly correlated electron system. [S0031-9007(97)02552-0]

PACS numbers: 71.30.+h, 75.30.Kz, 75.50.Ee

Materials showing a transition from a high temperature metallic to low temperature antiferromagnetic insulating phase, generally transition metal oxides, are sensitive to the relative value of the electronic bandwidth W and the intra-atomic Coulomb repulsion U [1]. These transitions are often loosely referred to as Mott-Hubbard transitions. In this paper we make reference to solutions of the Mott-Hubbard Hamiltonian for the case of intermediate frustration, considered in 1972 by Cyrot [2] and discussed recently by Kotliar and Moeller [3] and Moriya [3] among others, in which a metallic antiferromagnetic (AFM) phase is predicted for either low temperatures alone or intermediate between the high temperature magnetically disordered metallic (PMM) state and the low temperature antiferromagnetically ordered nonmetallic (AFI) state. Spalek and Wojcik [4] recently described an AFM phase and field induced metamagnetism using an almost localized fermion model. In this paper we show that the stoichiometric ternary ruthenate $Ca_3Ru_2O_7$, a $4d$ system having a tetragonal layeredlike structure and which is isostructural with the itinerant ferromagnet $Sr_3Ru_2O_7$ [5], undergoes a first-order metal to insulator transition and displays unique but predicted magnetic and transport properties at ambient pressure and without chemical substitution. Of most significance is the metallic antiferromagnetic phase (AFM) intermediate in temperature between the metallic paramagnetic phase (PMM, $T_N = 56$ K) and the low temperature nonmetallic antiferromagnetic phase (AFI, $T_M = 48$ K). The data presented here are for several well-characterized single crystals of $Ca_3Ru_2O_7$.

Experiments demonstrating the richness of phases associated with the classic Mott transition have to date been performed in $3d$ systems, mostly V_2O_3 and derivative systems, and have relied on controlled nonstoichiometric compositions, chemical substitution, or hydrostatic pressure to fine tune the properties [6]. A low temperature noncommensurate AFM phase was described recently in $V_{2-y}O_3$ for $0.015 < y < 0.04$ [6].

One of the most intriguing aspects of the metal-insulator transition is the mix of unusual magnetic order, enhanced electron interactions, and strong spin fluctuations that accompany the transition. The interplay of these elements bears on the ground-state properties of high-T_c cuprate superconductors, some giant magnetoresistive materials, and heavy fermion compounds. This recognition has led to a resurgence of interest in the metal-insulator transition in highly correlated electron systems primarily in $3d$ transition metal oxides such as the antiferromagnetic insulator La_2CuO_4 and its hole doped derivatives and in the Mott transition in the Brinkman-Rice correlated system V_2O_3. The three dimensional Mott-Hubbard Hamiltonian which contains the underlying physics continues to defy solution, and perturbative methods have not been successful in the critical region where W and U are comparable.

We present here the temperature dependence of the magnetization, $M(T, H)$ for $2 < T < 400$ K and $0 < H < 7$ T, isothermal magnetization for $5 < T < T_N$, electrical resistivity and its magnetic field dependence, $\rho(T, H)$ for $2 < T < 300$ K in dc fields to 30 T, and zero field heat capacity $C(T)$ for $1.5 < T < 20$ K. All experiments were performed on well-characterized single crystal samples, and data were often extracted separately from several single crystals to ensure integrity of the results. In both antiferromagnetic phases, $\rho(T, H)$ decreases sharply at well-defined metamagnetic transition fields determined from $M(T, H)$ [1]. The H-T phase diagrams constructed from transport and magnetic data are indistinguishable, and a multicritical point is identified at $T = 48$ T and $H = 4.1$ T.

Single crystals were grown in Pt crucibles using flux techniques from off-stoichiometric quantities of RuO_2, $CaCO_3$, and $CaCl_2$ (a self-flux). These mixtures were heated to 1480 °C in partially capped Pt crucibles, fired for 25 h, cooled at 2 °C/h to 1350 °C, and then rapidly cooled to room temperature. The resulting shapes of $Ca_3Ru_2O_7$ tend to be platelike with an average size of the single crystals being $1 \times 1 \times 0.4$ mm^3 with the c axis along the shortest dimension. The crystals used in this study were as grown. The starting ratio of Ca:Ru has a large influence not only on the form of crystals but also on the ratio of Ca:Ru in the crystals. The electrical resistivity was measured with a standard four probe technique and the magnetization with a commercial SQUID magnetometer.

$Ca_3Ru_2O_7$, which is isostructural with both $Sr_3Ru_2O_7$ and $Ca_3Ti_2O_7$, has a body-centered tetragonal crystal structure with the symmetry of $I4/mmm$ [7,8]. It is composed of pairs of closely coupled RuO_6 planes with the pairs offset along the c axis and separated by a layer of Ca and O ions. Results of SEM and EDX indicate that crystals studied are of high quality. X-ray diffraction patterns from powdered $Ca_3Ru_2O_7$ single crystals show no impurity peaks including $CaRuO_3$. The refinement of a body centered tetragonal cell using 31 reflections yielded $a = 3.841$ A and $c = 19.609$ A. The x-ray study suggests that the crystal structure of $Ca_3Ru_2O_7$ may be more distorted than the structure of $Sr_3Ru_2O_7$, due to the relatively smaller Ca ionic radius ($r_{Ca} = 1.0$ A), compared to Sr ($r_{Sr} = 1.18$ A). This may be similar to the case of $CaRuO_3$ and $SrRuO_3$ where the smaller Ca leads to the tilting of the RuO_6 octahedra, thus a more distorted perovskite structure than that for $SrRuO_3$ [9].

Shown in Fig. 1 are resistivity $\rho(2 < T < 300$ K) and magnetic susceptibility $\chi(5 < T < 400$ K, $H = 0.5$ T). (We determined that a field of 0.5 T was low enough to define "zero field" susceptibility.) The resistivity shows metallic behavior ($d\rho/dT > 0$) for $T > 56$ K and is relatively large (0.013–0.017 Ω-cm), indicating a narrow $4d$ band. A very abrupt first-order metal nonmetal transition T_M is seen at 48 K, followed by a rapid increase in $\rho(T)$ $[\rho(2\text{ K})/\rho(48\text{ K})] = 10$—a ratio which varies from 6 to 18, depending on samples. The data suggest a splitting, or at least partial Fermi surface gapping. The larger $\rho(T)$ along (001) is expected for a staggered layered system. Slight (001)/(100) anisotropy (not apparent in Fig. 1) is observed also for $T > T_M$ in the metallic phases. The resistivity $\rho(T)$ exhibits a small thermal hysteresis in the vicinity of T_M. This hysteresis, together with the abrupt $\chi(T)$ and $\rho(T)$ changes at $T_M = 48$ K, demonstrates that the transition is first order [1].

The susceptibility $\chi(T)$ below T_M drops precipitously, and far more rapidly than expected for a conventional antiferromagnet [10]. The drastically reduced $\chi(T)$ and its weak temperature dependence below T_M is reflective of strong exchange coupling or large anisotropy and resembles $\chi(T)$ behavior seen in V_2O_3 [6]. This may be due to a crossover from a three dimensional (3D) to a two dimensional (2D) coupling whose correlation length varies exponentially with temperature [11], but the origin of such behavior is unclear.

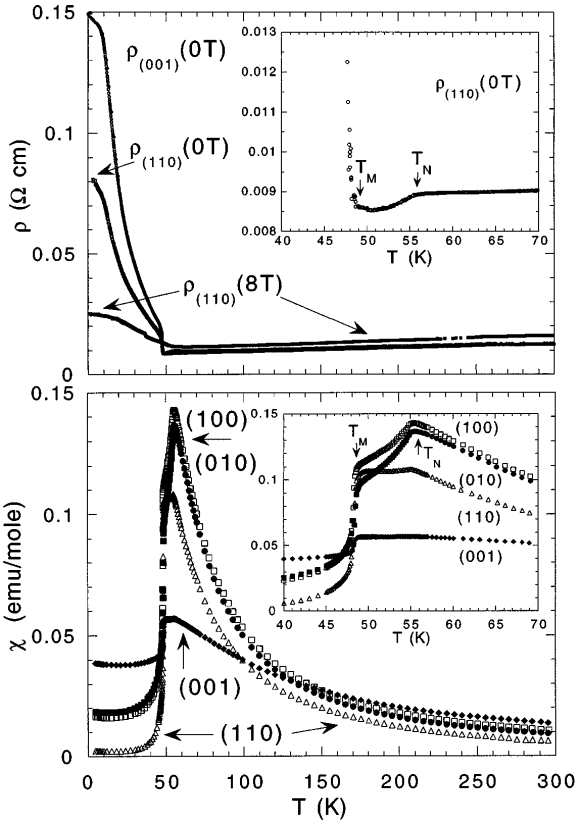

FIG. 1. Electrical resistivity $\rho(T)$ and magnetic susceptibility $\chi(T, H = 0.5$ T) as a function of temperature T. The insets show details of the two transitions.

For $48 < T < 56$ K there is a relatively weak but well-defined decrease in $\rho(T)$ (see the inset in the upper panel) which is like Fisher-Langer behavior [12]. This is followed by a small interval of T^2 dependence and below that a small increase in $\rho(T)$, which may be a precursor to the first-order transition at T_M. This would suggest that the energy difference between the phases at T_M is small for $T > T_M$. The metallic conductivity in the AFM phase persists for H to $4T$, though the rather abrupt decrease in $\rho(T)$ at $T = 56$ K shifts to lower T (terminating at 48 K), and it becomes less well defined.

In the PMM phase the anisotropy of $\chi(T)$ is unusually large, persisting up to 300 K. This anisotropy of $\chi(T)$ may be due to anisotropic exchange and/or strong but anisotropic electron correlations. Fitting $\chi(T)$ to a modified Curie-Weiss law, $\chi = \chi_0 + \chi/(T - \theta)$ for $150 < T < 390$ K yields the effective moment $2.42\mu_B$ for both (100) and (001) directions. The paramagnetic

Curie temperatures are $\theta = -67$ and -69 K, respectively, and χ_0, which is expected to roughly measure the density of states at the Fermi surface, is larger than in most metals. The effective moment may be compared to $2.83\mu_B$, expected for the $S = 1$ state of Ru [13]. These results are in accordance with those of specific heat (not shown) for $1.5 < T < 20$ K. The electronic specific heat coefficient determined from $C(T)$ is $\gamma = 37$ mJ/mol K^2. While γ, which is reproducible from sample to sample, is rather large, it is much smaller than some insulating heavy fermion systems, some of which, like $Ca_3Ru_2O_7$, show nonmetallic conductivity in the low temperature regime where γ is measured. In those systems γ results from localized electrons at the Fermi energy, or there may be partial gapping of the Fermi surface.

While $\chi(T)$ along (100) and (010) are nearly identical, $\chi(T)$ along (110) essentially vanishes for $T \ll T_M$, indicating that the moments lie antiferromagnetically coupled along (110). Recalling the crystal structure, moments may be coupled antiferromagnetically within all ab planes or ferromagnetically coupled within planes but antiferromagnetically between adjacent planes. The measured ratio of $\chi(T \ll T_M)$ for $H\|(001)$ vs $H\|(100)$ (ratio about $2^{1/2}$) is consistent with the (110)-aligned spin configuration. The metamagnetism data described below fully support the (110) spin configuration.

Shown in Fig. 2 are isothermal magnetization M and resistivity ρ as a function of applied magnetic field H. As seen in Figs. 2(a) and 2(b), there is a large jump in the moment at a critical field $H_{\rm cr}$. This appears to be a metamagnetic transition, and the anisotropic behavior between different directions is substantial. In Fig. 2(a), when $H\|(100)$ or (010), M not only shows a relatively broad transition at $H_{\rm cr}$ but is also unsaturated with a small moment ($\sim$0.7 μ_B/Ru at 15 K and 7 T), compared to $2\mu_B$ for the full $gS\mu_B$ moment [13]. In contrast, when $H\|(110)$, $M(T, H)$ [Fig. 2(b)] exhibits an extremely sharp transition at a lower $H_{\rm cr}$, and is completely saturated above $H_{\rm cr}$ with a nearly full ordered moment $1.73\mu_B$/Ru. These results together with the $\chi(T \ll T_N)$ show that the easy axis must be along (110).

For $40 < T < 48$ K a second transition at $H_{\rm cr2}$ appears which increases with temperatures (see inset). This two-step feature does not have the appearance of a spin flop transition. (The lower transition should occur at a field near $[2H_EH_A/(1 - a)]^{1/2}$, where H_E is the exchange field, H_A is the anisotropy field, and $a = \chi_\|/\chi_\perp$ [10]). The upper transitions are reminiscent of a flop-side two-step spin rotation seen, for example, in HoP [14]. Such transitions would require the anisotropy field to decrease with increasing temperature.

In Fig. 2(c) we show the large and sudden decrease in $\rho(H)$ at the corresponding $H_{\rm cr}$ for $H\|(110)$. This parallel change in both ρ and M indicates a strong coupling between charges and spin excitations, and thus possible formation of magnetic polarons where the charge carrier

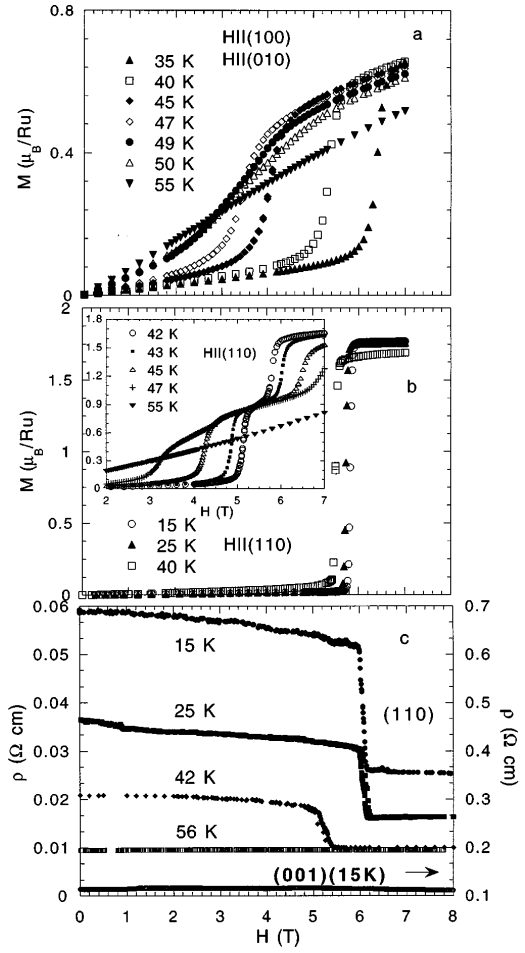

FIG. 2. Isothermal magnetization M and resistivity ρ as a function of applied magnetic field H. (a): $H\|(100)$ or (010): (b): $H\|(110)$; inset: $M(110)$ for $42 < T < 55$ K; (c): ρ for $H\|(110)$ (except as noted).

can move with its spin cloud. The coupling of $\rho(H)$ to $M(H)$ shown in Fig. 2 may be, in turn, interpreted in terms of a change in mobility μ $(= e\tau/m)$. This is to say, when $H < H_{\rm cr}$, the increased mass of the spin polaron reduces the mobility of charge carriers, resulting in localization. Conversely, when $H > H_{\rm cr}$, spins are rapidly aligned ferromagnetically, so no spin polarons form, and as a result, this increases the mobility and the conductivity. Such behavior has been observed in other systems, for example, the magnetic semiconductor EuTe [15]. An argument against the magnetic polaron is that there is no evidence for them, as they should give rise to a very low field jump in isothermal $M(H, T \ll T_N)$.

The magnetoresistance for $H\|(001)$ (lowest graph in Fig. 2) indicates no nonmetal to metal transition to $H = 10T$, consistent with (001) being the "hard" axis. We measured $\rho(4.2\ {\rm K}, H)$ with $H\|(001)$ in fields up to 30 T in the high dc field facility of the NHMFL and found a 7% decrease in $\rho(T = 4.2\ {\rm K}, H)$ by 30 T but no transition to the metallic PMM phase in this direction. The data

suggest some canting of the spins in the (001) direction out of the ab plane for H to 30 T.

Shown in Fig. 3 is the H vs T phase diagram derived from $M(T,H)$ and $\rho(T,H)$. When $H < 6$ T, $Ca_3Ru_2O_7$ evolves from PMM to AFM to AFI as temperature decreases. As H increases, the system becomes again a metal with spins aligned. This is labeled FMM(?) in the figure. The dashed line represents inflection points in the $M(T,H)$ data for $H > 6$ T (the second transition discussed above), and while we recognize this as a transition to full spin alignment, its relevance to the phase diagram, Fig. 3, is not clear. The confluence of the phase boundaries at $T = 48$ K and $H = 4.1$ T is a multicritical point. To the best of our measurements, the PMM/AFM phase boundary delineates second-order transitions and the other two boundaries first-order transitions.

We believe the results reported here for $Ca_3Ru_2O_7$ represent the first observation of the predicted PMM to AFM to AFI sequence of transitions. However, our understanding of these transitions is incomplete. The unusual behavior reflected in $Ca_3Ru_2O_7$ underscores its complexity but suggests a new class of oxide systems with which to explore the nature of the Mott-Hubbard-type problems. It is tempting to describe the AFM phase in terms of the almost localized Fermi liquid (ALFL) state discussed by Spalek and Wojcik [4] because the metamagnetic transitions in the AFM state are consistent with the ALFL theory. Most recently, Duffy and Moreo [16] described an AFM state for a two dimensional Mott-Hubbard model. Finally, Dobrosavljevic and Kotliar [17] describe a $T = 0$ partially filled Hubbard band model with disorder that gives rise to a Mott-Anderson transition which may have relevance to the data for $Ca_3Ru_2O_7$. Regardless of the interpretation, the AFM phase in $Ca_3Ru_2O_7$ stands alone as the most significant feature of this study.

We wish to thank J. Bolivar for assistance in the experiments and V. Dobrosavljevic, E Dagotto, and A. Moreo for discussions concerning the Mott-Hubbard model. The authors wish to acknowledge support provided by the National Science Foundation under Cooperative Agreement No. DMR95-27035 and the State of Florida.

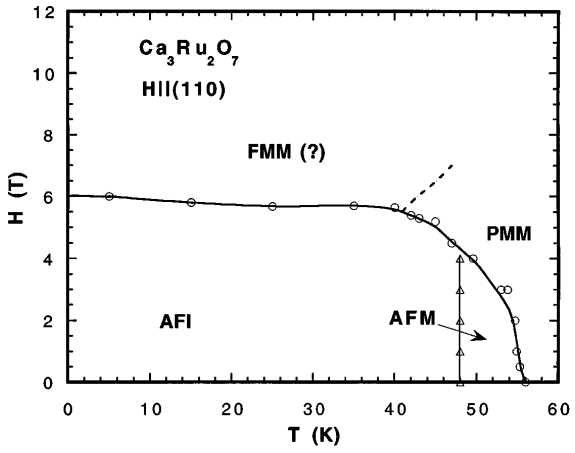

FIG. 3. H-T phase diagram derived from both $M(T,H)$ and $\rho(T,H)$. The dashed line represents inflections in isothermal $M(H)$.

*On leave at National High Magnetic Field Laboratory, Florida State University, Tallahassee, FL 32306. Also visiting scientist at Francis Bitter Magnet Laboratory, MIT, Cambridge, MA 02139.

[1] For a general review of the transition, see N. F. Mott, *Metal-Insulator Transition* (Taylor & Francis, London, 1990).
[2] M. Cyrot and P. Lacour-Gayet, Solid State Commun. **11**, 1767 (1972); J. M. D. Coey, Physica (Amsterdam) **91B**, 59 (1977).
[3] G. Kotliar and G. Moeller, in *Spectroscopy of Mott Insulators and Correlated Metals*, edited by A. Fujimori and Y. Tokura (Springer, Berlin, 1995), p. 15–27, and references therein; T. Moriya, *ibid.*, pp. 66–79.
[4] J. Spalek and W. Wojcik, in *Spectroscopy of Mott Insulators and Correlated Metals*, edited by A. Fujimori and Y. Tokura (Springer, Berlin, 1995), pp. 41–65.
[5] G. Cao, S. McCall, and J. E. Crow, Phys. Rev. B **55**, R672 (1997).
[6] S. A. Carter, T. F. Rosenbaum, P. Metcalf, J. M. Honig, and J. Spalek, Phys. Rev. B **48**, 16 841 (1993); S. A. Carter, T. F. Rosenbaum, M. Lu, H. M. Jaeger, P. Metcalf, J. M. Honig, and J. Spalek, Phys. Rev. B **49**, 7898 (1994); M. Takigawa, E. T. Ahrens, and Y. Ueda, Phys. Rev. Lett. **76**, 283 (1996); E. D. Isaacs, P. M. Platzman, P. Metcalf, and J. M. Honig, Phys. Rev. Lett. **76**, 4211 (1996); See also B. D. McWhan and J. P. Remeika, Phys. Rev. B **2**, 3734 (1970); D. B. McWhan, J. P. Remeika, T. M. Rice, W. F. Brinkman, J. P. Maita, and A. Menth, Phys. Rev. Lett. **27**, 941 (1971); W. Bao, C. Broholm, J. M. Honig, P. Metcalf, and S. F. Travino, Phys. Rev. B **54**, R3726 (1996).
[7] H. K. Muller-Buschbaum and J. Wilkens, Z. Anorg. Allg. Chem. **591**, 161 (1990).
[8] S. N. Ruddlesden and P. Popper, Acta Crystallogr. **11**, 54 (1958).
[9] W. Bensch, H. W. Schmalle, and A. Reller, Sold State Ionics **43**, 171 (1990).
[10] S. Foner, J. Appl. Phys. **39**, 411 (1968).
[11] T. Thio, T. R. Thurston, N. W. Preyer, P. J. Picone, M. A. Kastner, H. P. Jenssen, D. R. Grabbe, C. Y. Chen, R. J. Birgeneau, and A. Aharony, Phys. Rev. B **38**, 905 (1988); E. Manousakis, Rev. Mod. Phys. **63**, 1 (1991).
[12] M. E. Fisher and J. S. Langer, Phys. Rev. Lett. **20**, 665 (1968).
[13] For example, see J. B. Goodenough, Prog. Solid State Chem. **5**, 145 (1971).
[14] H. R. Child, M. K. Wilkinson, J. W. Cable, W. C. Koehler, and E. O. Wollan, Phys. Rev. **131**, 922 (1963).
[15] Y. Shapira, S. Foner, N. F. Oliviera, and T. B. Reed, Phys. Rev. B **5**, 2647 (1972).
[16] D. Duffy and A. Moreo (to be published).
[17] V. Dobrosavljevic and G. Kotliar (to be published).